The Cryosphere Discuss.,
https://doi.org/10.5194/tc-2020-181-AC1, 2020

The Cryosphere Discussions

Interactive comment on "Mapping seasonal glacier melt across the Hindu Kush Himalaya with time series SAR" *by* Corey Scher et al.

Corey Scher et al.

nsteiner@ccny.cuny.edu

Received and published: 30 November 2020

Reviewer 1: General comments

This manuscript discusses the use of time series of Sentinel-1 SAR imagery to map regional melt characteristics of glacier ablation in the Hindu Kush Himalaya region.The topic is of high importance to further understand how to operationally use Sentinel-1 SAR backscatter intensity for mapping glacier characteristics. The authors are using the SAR data to investigate the duration of seasonal glacier melt,these are important inputs to surface energy models. Additionally,using time series SAR data is of high importance for further under-

standing of how to map glaciers using SAR backscatter signals, e.g. refreezing of liquid water in the percolation zone.

The authors give a good overview of the regional glacier melt dynamics in the HKH region and this is a very interesting study. However, the presented results are rather general in terms of the regions studied and lacks a proper error analysis.The Text has some long and complex sentences here and there, but is overall relatively easy to understand.

We thank the referee for careful review of our work and thoughtful suggestions for improvement. We have conducted major revisions detailed in the responses below. We include all updated figure captions in the response text.

Specific comments

The chapter about SAR processing (2.3 Computer Infrastructure) is too limited, e.g. there are many processing options in SNAP that are not described properly. To be able to reproduce the data, more information about the processing of Sentinel-1 satellite images is thus needed.

Author response (AR) 1: We agree that the section was limited and will modify Section 2.3 as follows; and welcome any further suggestions:

Computing Infrastructure

A cloud-computing platform and application programming interface with pre-processed radiometrically terrain corrected Sentinel-1 A/B data was used to detect melt characteristics across the region (Gorelick, Hancher et al. 2017). Radiometric terrain

correction of Sentinel-1 data was conducted upon ingestion to the cloud server using the ESA's method contained within the Sentinel Applications Platform (SNAP) processing toolbox (ESA). The SNAP toolbox is used for processing of Sentinel-1 images and through a stepwise process of updating orbit metadata with restituted orbit files, removal of invalid edge data and low intensity noise, removal of thermal noise, computation of backscatter intensity, and finally orthorectification (Google 2020). The SNAP toolbox terrain correction functionality utilizes the 30m spatial resolution SRTM DEM (Farr 2007, Margulis, Liu et al. 2019). The pre-processed SAR times series data and API functionality used to derive glacier melting characteristics are available from GEE and can be used to recreate the work presented in this study.

The authors should also be aware of the limitations of the SRTM DEM over glaciers used here for processing the Sentinel-1 data (e.g. Kääb, A., Treichler, D., Nuth, C., and Berthier, E.:Brief Communication: Contending estimates of 2003–2008 glacier mass balance over the Pamir–Karakoram–Himalaya, The Cryosphere, 9, 557–564, https://doi.org/10.5194/tc-9-557-2015, 2015.).

AR2: We are aware of the bias in SRTM DEMs caused by the depth of penetration using C-band observations to determine the surface height. Additional errors associated with using SRTM in complex terrain extend beyond C-band penetrations. More error is associated with shadowing and foreshortening. Hence the gap filling performed using the SRTM 30m DEM. However, the radar signal associated with melting is large and well above any variability in normalized backscatter from errors in terrain correction. Since we are selecting time-series with constant viewing geometry, not normalizing to a constant incidence, the errors from SRTM should be consistent within each pixel. We acknowledge that by using elevation bins from the SRTM DEM to calculate summary statistics over climate subregions of the HKH our results may be biased towards higher elevations. Based on prior work, we estimate this bias will be less than

10 m on average (Gardelle, 2012).

Reviewer Comment: Unfortunately, the authors do not give detailed error estimates in relation to the Sentinel-1 SAR time series over glacier ablation. The study lacks in situ observations for comparison with the SAR backscatter intensity, and the authors should discuss whether the results are trustworthy in the HKH-region.

AR3: We agree with the reviewer's comment, it would be ideal to provide a detailed and spatially resolved estimate of error for our surface melting observations. However, it is a well known problem that observational data at high elevations, and especially in High Mountain Asia (HMA), are severely lacking. For this reason it is vital that remote sensing is used to address deficiencies in observation, rather than being reliant on surface stations. We contend that time series synthetic aperture radar (SAR) instruments are ideally suited to measure glacier melting, in some cases better than using weather station measurements such as air temperature alone. We provide evidence of this point below.

There is an extensive record of research focused on radar applications to surface melting observation over glaciers and ice-sheets in polar regions (e.g., (Shi and Dozier 1995, Ashcraft and Long 2001, Ashcraft and Long 2007, Trusel, Frey et al. 2013, Steiner and Tedesco 2014)). It is clear that surface melting over glaciers produces a very strong and very well understood radar signal that is well established in radiative transfer theory (Ulaby and Stiles 1980). As indicated in the manuscript Figure 4 (Figure AR2, below) this melting response is measured commonly at 20x the variance of the baseline reference state (winter) and at almost always over 5x. Second, backscatter signals associated with glacier melting are unambiguous in time series observations over ice and snow, there are few seasonal phenomena that create confusion in radar melt-detection approaches. Because of this, SAR time-series observations of surface

melting are used by Johnson et al. (2020) as sources of validation and calibration for surface melting estimates in areas where surface measurements are not practical (Johnson, Fahnestock et al. 2020).
To better demonstrate the utility of radar backscatter for characterizing surface melting we have added a comparison with newly-available surface meteorology measurements from the Mt. Everest region. Automated weather stations (AWS) were installed by the National Geographic Everest Expedition and detailed in Matthews, et al. (2020) (Matthews, Perry et al. 2020). We estimate periods of surface melting from the full surface energy balance (SEB) at the surface using these stations (Figure AR1). We find that Sentinel-1 melt classifications detect SEB estimates of surface melting at the Everest Camp II AWS (6464m a.s.l.) and with an accuracy score that ranges from 73 to 85 percent and from 63 to 68 percent at Mt. Everest South Col (7945m a.s.l.) depending on the parameterization of surface roughness used in SEB estimates of melting. In these locations the average daily temperature never exceeds 0oC, degree day estimates of surface melting would not indicate melting in either station. We find that the S1-SAR finds 80 to 133 days of melting at Mt. Everest Camp II while the SEB indicates 100 days. At Mt. Everest South Col the S1-SAR finds either 19 or 77 days of melting while the SEB indicates 56. This analysis and discussion of the results will be added to the manuscript.
Based on comparisons with SEB modeling, and the physical basis of SAR measurements we have a high degree of confidence in our methodology and in the ability of the SAR backscatter to detect melting and in data-poor regions such as HMA remote sensing records of this type provide vital information supporting the understanding of surface melt on mountain glaciers. This is crucial to understand SEB on glacier and associated links to climate and downstream hydrological and ecological processes (Kayastha, Steiner et al. 2019).

Figure AR1. Air temperature measurements from (a) the Everest Camp II automated weather station (AWS) and (b) the Mt. Everest South Col AWS are compared to glacier

surface melting observations from the Sentinel-1 satellite synthetic aperture radar (SAR). (c) The radar backscatter from the Khumbu Glacier (at 6483 m a.s.l.) adjacent to the Camp II AWS, show a pronounced decrease in backscatter over several months associated with on-going surface melting during summer months. Melting is identified when backscatter decreases below a threshold (dashed-line), set at 3 dB below the winter mean (solid-line). (d) At the upper reaches of the Khumbu Glacier (7128 m a.s.l.), S1-SAR observes melting during ascending passes (18:00 local time) but not during descending passes (06:00 local time) except for a brief period during late June. (e, f) Timing of surface melt from observation and SEB modeling (Matthews et al., 2020) are compared to S1-Asc and Dsc observations at Camp II and South Col AWS, respectively. The cumulative number of melting days from the SEB model and S1-SAR (g, h)

... Even though in situ measurements might be absent, the authors might compare the melt signals retrieved from Sentinel-1 SAR data to other remote sensing sources (optical e.g. Landsat-8 and/or Sentinel-2 and SAR e.g. Radarsat-2).
AR4: Current sources of thermal infrared measurements lack either the resolution (MODIS, AVHRR) or the temporal repeat (Landsat, Sentinel-2) to fully validate our surface melting product. Also, thermal infrared observations are somewhat limited by atmospheric effects (e.g. moisture, clouds), leading to uncertainties in determining the temperature at the surface under uncertain or indeterminate (unmeasured) weather conditions in HMA. Microwave sensors, e.g. SAR and radiometers are considered the best available option for detecting thaw and melt onset associated with the presence of liquid water (Entekhabi, Njoku et al. 2010). As stated previously, SAR backscatter responds to the liquid water content of the snow directly, rather than surface temperature. This backscatter response is pronounced and unambiguous. Although it would be interesting to explore the combined efficacy of thermal infrared and radar backscatter for characterization of mountain glaciers, thermal infrared observations do not provide a suitably robust standard for validating melt events characterized

by microwave SAR. A full comparative analysis is beyond the scope of this current manuscript and recommended for future research.

The four glacier regions studied are rather large, and it would have been interesting to understand more of the local variations of backscatter intensity values within these regions. A suggestion is to pick out some glaciers from each region and compare results from these individual glaciers.
AR5: We fully agree with the reviewer and have reconstructed the summary statistics by glacio-climatic region of HMA detailed in Bolch, et al (2019) (Bolch, Shea et al. 2019). Plots of z-score by elevation for each su-bregion. Please see the new figure below (Figure AR2).

Figure AR2. (Top) Glacio-climate subregions within the Hindu Kush Himalaya delineated in Bolch et al. (2019). (Middle) Mean z-score (2017-2019) by 100m SRTM elevation bin over each sub-region in the HKH. (Bottom) Mapped glacier area from the GAMDAM database (Sakai, 2019) over 100m SRTM (Farr 2007) elevation bins for each subregion.

If possible, the authors should discuss the refreezing process in the percolation zone in the Hindu Kush Himalaya region in more detail.
AR6: We agree that discussion of percolation zone backscatter signatures are limited and, with new analyses by glacio-climatic subregion used to summarize melt retrievals, we believe that the Results and Discussion section, along with subsection 4.1 on percolation zone meltwater and radar backscatter, could benefit from some restructuring. We propose a restructuring of the entirety of section 4 (Results and Discussion) and 4.1 (Percolation Meltwater Hydrology) as follows:

Discussion
A melting signal ($z > 2$) is observed across 97% (62,907 km2) of the mapped glacier area contained in the GAMDAM inventory. Melt retrievals are aggregated across 12 glacio-climate subregions within the HKH delineated by Bolch et al. (2019) and averaged across the calendar years 2017-2019 to report summary statistics. Aggregate statistics of melt onset (MO) and freeze onset (FO) are calculated across 100m elevation bins using the 30m SRTM (Farr 2007)digital elevation model for each glacio-climate subregion as presented in Figure AR3. For all subregions, there is a roughly linear relationship of mean MO with elevation over most elevations. The progression of MO with increasing elevation is consistent with lapse rate temperature controls on surface melting for most elevation ranges. Notably, we find an inflection toward earlier melt onset occurring at higher elevations (>6,500m a.s.l.). A divergence from lapse-rate driven melting at high elevations suggests that snowmelt onset may have regional triggers, like strong solar insolation (Matthews et al., 2019) or variable regional weather patterns; such as increases in atmospheric moisture, cloudiness, and deep convection induced by absorbing aerosols (Lau, Kim et al. 2010). In the three years of freeze onset (FO) across subregions we do not find the level of elevation dependence as observed in melt MO (Fig. AR3). For much of the HMA, FO occurs during a short period of time and over large spans of elevation. For example, in the Central Himalaya subregion, FO spans an average of 37 days while the MO for this region spans 78 days on average. Freeze onset (FO) across subregions does not follow a linear trend with elevation similar to melt MO (Fig. AR3). In western subregions (Eastern Hindu Kush, Western Pamir, and Karakoram), there is a signal of delayed refreeze apparent in summary statistics at higher elevation ranges within each respective catchment (Supplementary Fig. 1). In the Western Pamir, FO at 6,000m occurs 22 days later than FO at 5,000m a.s.l. Similarly, in the Karakoram, FO occurs 10 days later on average at 7,500m a.s.l. compared to 6,500m a.s.l. In the Tanggula Shan, FO at 6,500m a.s.l. is delayed by 21 days relative to FO at 5,500m a.s.l. (Supplementary Fig. AR1). Signals of delayed refreeze are observed at elevation ranges similar to greatest z-score across

each subregion (Supplementary Fig. AR1). Complete refreeze across the depth of a percolation zone is delayed relative to percolation zone surfaces because liquid water is retained within a percolation zone media after the surface of the percolation zone has frozen (Paterson 2016). Completely frozen percolation zones produce some of the largest radar backscatter responses on the terrestrial earth (Jezek, Gogineni et al. 1994). Because frozen snow and percolation facies are essentially transparent, C-band SAR will be sensitive to the presence of liquid water across the volume of a snowpack or firn strata (Fischer, Jäger et al. 2019). Signals of delayed refreeze across subregions are indicative of meltwater storage within the percolation volume due to meltwater retention (Supplementary Fig. AR1).

Figure AR3. Melt onset (MO) and freeze onset (FO) summarized in 100m elevation bins using the 30m SRTM digital elevation model (Farr 2007) and 12 glacio-climate subregions (Bolch, 2019).

Supplementary Fig 1. Melt onset (MO), freeze onset (FO), and z-score averaged over 100m elevation bins using the 30m SRTM digital elevation model (Farr 2007) and delineations of 12 glacio-climate subregions identified in Bolch, et al. (2019). Z-score maxima across subregions largely correspond to elevation ranges of delayed refreeze.

Percolation Meltwater Hydrology

Delayed freeze-up apparent in summary statistics at unique elevation ranges across glacio-climate subregions is an important illustration of how melt retrievals from Sentinel-1 are sensitive to the presence of liquid water across the depth of snowpack and/or firn (Brangers, Lievens et al. , Fischer, Jäger et al. 2019). At the Khumbu glacier on Mount Everest, Sentinel-1 retrieved refreeze occurs over thirty days later at 6,000m a.s.l. compared to elevations below 5,400m a.s.l. and above 6,200m a.s.l., indicating that liquid meltwater was retained at elevation ranges between

5,400-6,2000m a.s.l. during a month when elevations both above and below this range were recorded as completely frozen within Sentinel-1 retrieved melt signals. The time series of mean Sentinel-1 SAR backscatter for descending orbital nodes from two 250m buffered points on the Khumbu glacier show a rapid increase in SAR backscatter magnitude for the higher elevation location, whereas backscatter time series extracted from within the elevation range of delayed melt offset show a gradual increase in radar backscatter. We interpret this gradual strengthening of the backscatter signal to be indicative of gradually decreasing liquid water content in the snowpack (or firn) as refreeze progresses from the glacier surface and into the depth of the percolation zone (Fig. AR4) (Forster et al., 2014; Miège et al., 2016). This elevation range (5,400-6,200m a.s.l.) is similar to known elevation ranges of percolation zones on the Khumbu glacier as detailed in recent field work (Matthews, Perry et al. 2019, Matthews, Perry et al. 2020). SAR backscatter data showing a gradual increase in backscatter within the region of a known percolation zone suggests that there may exist a relationship between frozen percolation zone depth and C-band backscatter intensity across refreeze cycles; where C-band backscatter gradually increases with frozen percolation zone depth during a refreeze process.

Figure AR4. (Top) Refreeze timing over Khumbu glacier region of Mount Everest in the Central Himalaya. Red regions of freeze onset occur at mid-elevations, indicative of delayed refreeze due to meltwater retention in percolation zones. (Bottom) Sentinel-1 backscatter time series from two points on the Khumbu glacier, one within known elevations of glacier percolation facies (teal square, 6,000m a.s.l.) and another point at elevations where temperatures likely do not exceed 0°C annually (pink triangle, 6,600m a.s.l.).

L 70, P 3: "This study builds on extensive research into microwave scattering from dry and wet snow and techniques for snowmelt retrieval from imaging

radar sensors to present an operational monitor for spatially-resolved glacier surface melt characteristics using synthetic aperture radar (SAR) time series and up-to-date glacier outlines derived from satellite optical imagery across the HKH." Which years are the up-to-date glacier outlines from? (Sakai, 2019)

AR8: Glacier outlines were updated using data from the Landsat archive spanning 1990-2010. We suggest adding information on the sourcing of the glacier outlines by changing L 70 P 3 to read:

"The recently recently updated glacier outlines were derived from satellite optical imagery captured across the HKH by the Landsats 5 and 7 between 1990-2010 (Sakai, 2019)."

L 85, P 3: "In areas that are seasonally snow-free, like for areas of debris-cover or bare ice, melting conditions are dominated by surface scattering that is significantly darker relative to winter conditions (Lievens et al., 2019)." What is meant by "darker"? Is this connected thoroughness differences between debris-cover, bare ice and wet snowshoeing different backscatter intensity?

AR 9: We acknowledge that this phrasing is unclear and propose to change L 85, P3 as follows:

"In areas that are seasonally snow-free, like ablation zone debris-covered or bare ice surfaces, melting conditions are dominated by surface scattering once snowpack has completely melted away, which produces Sentinel-1 VH imagery with significantly lower backscatter intensity, causing SAR backscatter images to appear much darker over these zones when the glacier surface is no longer snow-covered relative to winter

conditions of deep and frozen snowpack (Lievens et al., 2019)"

L 95, P 4: "Limited only by the frequency of observations (12-days per orbit direction)". Are 6-days repeat orbits of Sentinel-1 available in the study region? If not, will 6-days repeat be available in the future? If so, this should be discussed.
AR 10: We will add the following discussion following L95, P4:

Six-day repeat orbits are only available by combining ascending and descending paths. Because of the complexity of the terrain and varying look angles by orbit direction and relative orbit cycle number, we restricted SAR processing to distinct orbit directions and chose the orbit cycle and direction with greatest annual z-score in order to select an orbit direction and orbit cycle to choose for melt classification. If we attempted to combine orbit directions, our derived product would have inconsistent temporal resolution, as some orbit paths and directions pass the z-score criteria but in other regions only one orbit direction will capture the melt signal due to the complexity of the terrain. For the purposes of maintaining consistency throughout the derived dataset, we restricted to choosing only one orbit direction and one orbit pass within that direction to classify melt per pixel, which results in melt retrievals of 12-day resolution.

L 155-160, P 7: Why only Sentinel-1 SAR imagery from 2017-2019? Sentinel-1A was operative since 2014.
AR 11: We will add the following sentence after L154, P7:

Cross-polarized Sentinel-1 SAR did not become available over the HKH until early 2017 and thus restricted this study timeframe.

L 160, P 7: "By combining orbit directions, we utilize observations acquired at day and night. For the purpose of this study we do not attempt to resolve diurnal-scale melt freeze processes and instead focus on retrieving annual characteristics of melt timing and duration." The backscatter intensity signal differs between day and night. Further explanation on how this might affect the results must be included.
AR 12: The backscatter intensity signal will only vary significantly as refreeze processes progress within the snowpack and percolation areas. For the purposes of determining freeze/thaw status across a snowpack on a glacier surface, the retention of meltwater in the snow, and resulting snow wetness, is understood to persist until complete refreeze has taken place (Samimi and Marshall 2017). At C-band frequencies, this snow wetness will be visible across the volume of the snowpack (or firn strata) and diurnal refreeze processes that may be active at the surface of the glacier will not alter retrievals of wet snow across the volume.

L 261, P11: "Mean seasonal melt magnitude averaged over 100m elevation bins over all three calendar years of data shows strong ($z > 2$) melt signals across glacio-climatic sub-regions and across all elevation ranges of significant glaciation (Fig. 4). The occurrence of seasonal melt signals across all ranges of elevation in the HKH is both noteworthy and striking." These statements should be placed in the Results and Discussion section.
AR 13: These sentences will be moved accordingly.

L 315, P 14: "A summary of glacier melt timing with elevation averaged across study years is shown across 100m elevation bins in Figure 5 and tabulated across 1 km elevation bins in Table 2. Due to errors in melt classification at elevations below 3,500m a.s.l., we will summarize our observations across elevations >3,500m a.s.l. and assume that the relatively small glaciated area at

elevations at or below 3,500m a.s.l. is negligible for the purposes of identifying trends across regions and elevation." What kind of errors are referred to? And What are the assumptions based on?
AR 14: We hypothesize that erroneous melt classification at low elevations is due to combined effects of a shallow seasonal snowpack and heterogeneities across ablation zone surfaces (like debris-cover, sun-cups, supra-glacier meltwater, etc.), complicating radar backscatter returns to the sensor. Since less than 2% of glacier area exists at elevations less than 4,000m a.s.l. We believe that sparse results at the lowest glaciated elevations should not inhibit the interpretation of the dataset across regions with pronounced melt signals ($z > 2$).

Technical comments

Figure 1: Top: Glacier outlines are not that apparent in the figure. Bottom: Blue color of descending swaths would be clearer.
AR 15: To illustrate the number of glaciers within glacio-climatic subregions of the HKH, in Figure 1 we summarized the total glacier area by subregion and highlighted some of these glacier outlines with an inset map. We have also changed the colors of the descending swath paths to blue.

Figure AR5. (Top) Hindu Kush Himalaya (HKH) region and 2018 GAMDAM glacierized areas summed across glacio-climate subregions from Bolch, et al. (2019). An inset map highlights the spatial fidelity of GAMDAM outlines in the top panel. GGI and HKH data are overlaid onto a 30m 135Shuttle Radar Topography Mission (SRTM) DEM hillshade (Farr 2007). (Bottom) Sentinel-1 ascending (red) and descending (blue) swath footprints acquired across the study region. Ascending orbit cycle number 56 is highlighted in red to illustrate the SAR image processing approach for time series analysis across distinct orbit cycles.

Figure 2: Figures are too small and dark, and are hard to interpret. A suggestion is to cut down on the amount of figures and enlarge the most important ones that indicates VH polarization which is used in this work. Consider a brighter color on glacier outlines.

AR 16: We have cut down on area in these figures and highlighted the VH polarization, per your suggestion.

Figure AR6. (A) Mean summer (July-August) 2018 cross-polarized (VH) backscatter across an example region in the Trishuli basin, Nepal. (B) Mean 2018 winter (January-February) VH backscatter from Sentinel-1. (C) Sentinel-2 false-color (near-infrared, green, blue) image acquired by Sentinel-2 on October 30, 2018. Glacier outlines are shown in blue and the Yala glacier base camp meteorological station is marked in red. Note the snow covered and bare-ice portions of outlined glaciers and other debris-covered portions of glacier ablation areas. (C) The difference between mean summer and winter VH backscatter from Sentinel-1.

Figure 3: Use same scale in the plots for VV and VH backscatter.
AR 17: We have changed the plot to include both polarizations on the same color scaling.

Figure AR7. Time-series chart of air temperature measured at the Yala glacier base camp (4,950m a.s.l) andSentinel-1 A/B descending backscatter averaged across the Yala glacier for the years 2017-2018. Assessment of algorithm performance assuming mean daily air temperatures above 0°C indicates active melt results in 96% accuracy for melt classification across this time series in the VH polarized backscatter.

Figure 5: Suggestion to have elevation on the y-axis. Make the plots broader so more information can be interpreted. Include stippled lines for each 50 DOY in the figure to help the reader to interpret the results.

AR18: We have swapped the axes on these plots after re-running the analysis using glacio-climatic sub-regions delineated in Shean, et al. (2019) and have also created a supplementary figure (Supplementary Fig. AR1) to highlight melt retrievals and z-scores within each subregion.

Figure AR8. Melt onset (MO) and freeze onset (FO) summarized in 100m elevation bins using the 30m SRTM digital elevation model (Farr 2007) and 12 glacio-climate subregions (Bolch, 2019).

Figure 6: Difficult to understand and interpret the small circular insertions in the plot. Make them larger and explain more carefully, if these are of big importance.

AR 19: We split the inset maps into a separate figure: one to highlight the results of the melt retrieval algorithm presented in this work, and another to summarize melt retrievals across subregions delineated in Shean, et al. (2019).

Figure AR9. Melt retrievals averaged over the calendar years 2017-2019 in the Central Himalaya and Karakoram regions. (A) Mean melt onset (DOY) in the Khumbu glacier region of the Central Himalaya. (B) Mean melt onset (DOY) over the Siachen glacier in the Karakoram region. (C) Mean melt offset (DOY) in the Khumbu glacier region of the Central Himalaya. (D) Mean melt offset (DOY) over the Siachen glacier

in the Karakoram region.

Figure AR10. Melt onset (top) and freeze onset (bottom) averaged over 2017-2019 plotted over a SRTM 30m DEM hillshade (Farr 2007). Melt retrievals are averaged across glacio-climate subregions identified in Bolch, et al. (2019) and scaled by the mapped glacier area within each subregion.

Figure 8: Suggest to show the location on a map and include glacier outlines.
AR 20: We have added an inset map to Figure 8.

References should be in chronological order. e.g. L72, P
AR 21: We will restructure references to make sure they are in chronological order.

References for Author Response 1

Ashcraft, I. S. and D. G. Long (2001). Azimuth variation in microwave backscatter over the Greenland ice sheet. IGARSS 2001. Scanning the Present and Resolving the Future.

Proceedings. IEEE 2001 International Geoscience and Remote Sensing Symposium (Cat. No. 01CH37217), IEEE.

Ashcraft, I. S. and D. G. Long (2007). "Comparison of methods for melt detection over Greenland using active and passive microwave measurements." International Journal of Remote Sensing 27(12): 2469-2488.

Bolch, T., J. M. Shea, S. Liu, F. M. Azam, Y. Gao, S. Gruber, W. W. Immerzeel, A. Kulkarni, H. Li and A. A. Tahir (2019). Status and change of the cryosphere in the Extended Hindu Kush Himalaya Region. The Hindu Kush Himalaya Assessment, Springer: 209-255.

Brangers, I., H. Lievens, C. Miège, M. Demuzere, L. Brucker and G. De Lannoy "SentinelâĂŘ1 detects firn aquifers in the Greenland Ice Sheet." Geophysical Research Letters.

Entekhabi, D., E. G. Njoku, P. E. O'Neill, K. H. Kellogg, W. T. Crow, W. N. Edelstein, J. K. Entin, S. D. Goodman, T. J. Jackson and J. Johnson (2010). "The soil moisture active passive (SMAP) mission." Proceedings of the IEEE 98(5): 704-716.

Farr, T. G., Rosen, P.A., Caro, E., Crippen, R., Duren, R., Hensley, S., Kobrick, M., Paller, M., Rodriguez, E., Roth, L., Seal, D., Shaffer, S., Shimada, J., Umland, J., Werner, M., Oskin, M., Burbank, D., and Alsdorf, D.E. (2007). "The shuttle radar topography mission: Reviews of Geophysics, v. 45, no. 2, RG2004, at https://doi.org/10.1029/2005RG000183." Reviews of Geophysics 45(RG2004).

Fischer, G., M. Jäger, K. P. Papathanassiou and I. Hajnsek (2019). "Modeling the Vertical Backscattering Distribution in the Percolation Zone of the Greenland Ice Sheet with SAR Tomography." IEEE Journal of Selected Topics in Applied Earth Observations and Remote Sensing 12(11): 4389-4405.

Google. (2020). "Sentinel-1 Preprocessing." Retrieved Novermber 30, 2020, 2020, from Sentinel-1 Preprocessing.

Gorelick, N., M. Hancher, M. Dixon, S. Ilyushchenko, D. Thau and R. J. R. S. o. E. Moore (2017). "Google Earth Engine: Planetary-scale geospatial analysis for everyone." 202: 18-27.

Jezek, K. C., P. Gogineni and M. Shanableh (1994). "Radar measurements of melt zones on the Greenland ice sheet." Geophysical Research Letters 21(1): 33-36.

Johnson, A., M. Fahnestock and R. Hock (2020). "Evaluation of passive microwave melt detection methods on Antarctic Peninsula ice shelves using time series of Sentinel-1 SAR." Remote Sensing of Environment 250: 112044.

Kayastha, R. B., N. Steiner, R. Kayastha, S. K. Mishra and K. McDonald (2019). "Comparative study of hydrology and icemelt in three Nepal river basins using the glacio-hydrological degree-day model (GDM) and observations from the Advance Scatterometer (ASCAT)." FrEaS 7: 354.

Lau, W. K., M.-K. Kim, K.-M. Kim and W.-S. Lee (2010). "Enhanced surface warming and accelerated snow melt in the Himalayas and Tibetan Plateau induced by absorbing aerosols." Environmental Research Letters 5(2): 025204.

Margulis, S. A., Y. Liu and E. Baldo (2019). "A joint Landsat-and MODIS-based re-analysis approach for midlatitude montane seasonal snow characterization." Frontiers in Earth Science 7: 272.

Matthews, T., B. Perry, D. Aryal, D. Shrestha and A. Khadka (2019). New Heights in Glacier-Climate Research: Initial Insights From the Highest Weather Stations on

Earth. AGU Fall Meeting 2019, AGU.

Matthews, T., L. B. Perry, I. Koch, D. Aryal, A. Khadka, D. Shrestha, K. Abernathy, A. Elmore, A. Seimon and A. Tait (2020). "Going to Extremes: Installing the World's Highest Weather Stations on Mount Everest." Bulletin of the American Meteorological Society. Paterson, W. S. B. (2016). The physics of glaciers, Elsevier.

Samimi, S. and S. J. Marshall (2017). "Diurnal cycles of meltwater percolation, refreezing, and drainage in the supraglacial snowpack of Haig glacier, Canadian Rocky Mountains." Frontiers in Earth Science 5: 6.

Shi, J. and J. Dozier (1995). "Inferring snow wetness using C-band data from SIR-C's polarimetric synthetic aperture radar." IEEE transactions on geoscience and remote sensing 33(4): 905-914.

Steiner, N. and M. Tedesco (2014). "A wavelet melt detection algorithm applied to enhanced-resolution scatterometer data over Antarctica (2000–2009)." The Cryosphere 8(1): 25-40.

Trusel, L. D., K. E. Frey, S. B. Das, P. K. Munneke and M. R. Van Den Broeke (2013). "SatelliteâĂŘbased estimates of Antarctic surface meltwater fluxes." Geophysical Research Letters 40(23): 6148-6153.

Ulaby, F. T. and W. H. Stiles (1980). "The active and passive microwave response to snow parameters: 2. Water equivalent of dry snow." Journal of Geophysical Research: Oceans 85(C2): 1045-1049.

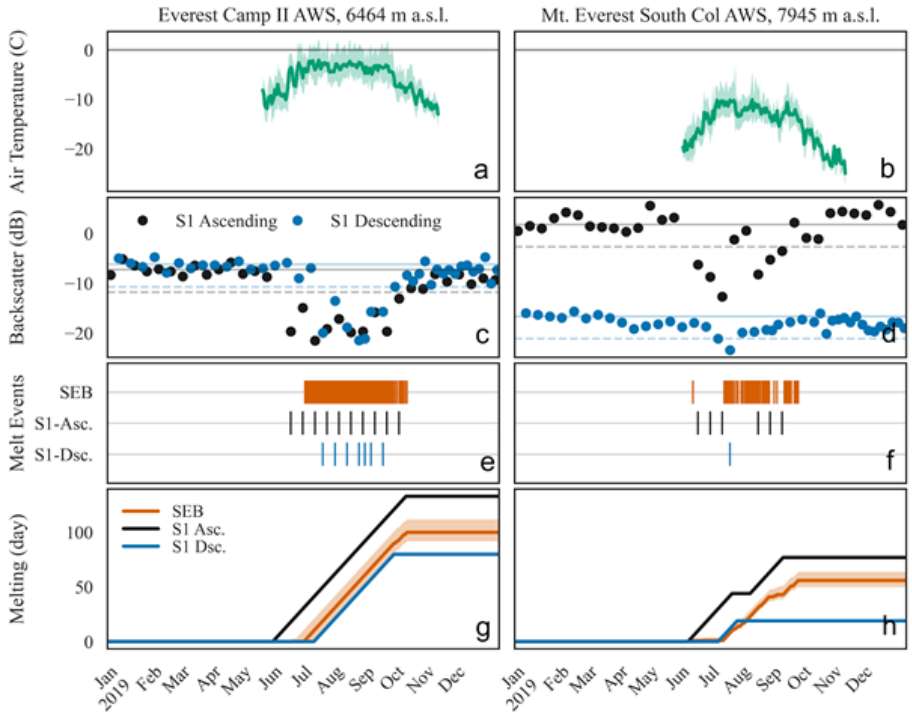

Fig. 1. Figure AR1. Please see text for caption.

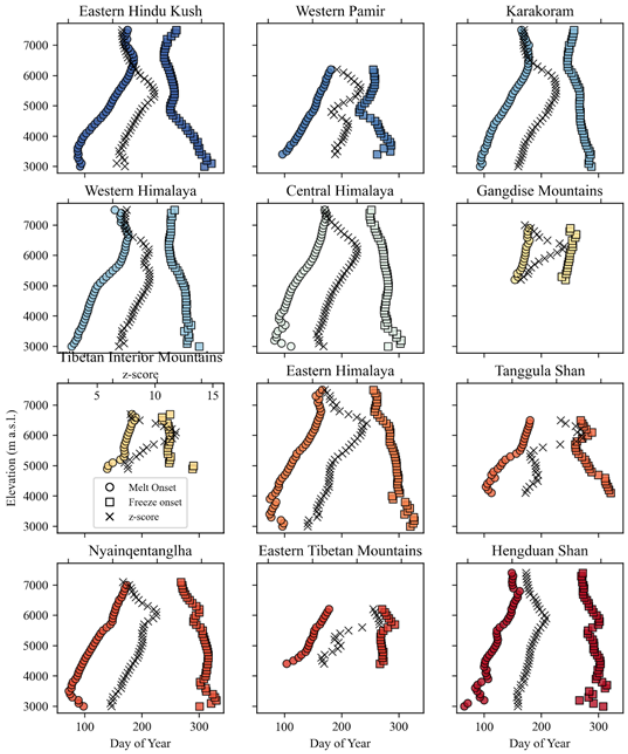

Fig. 2. Supplemental Figure 1

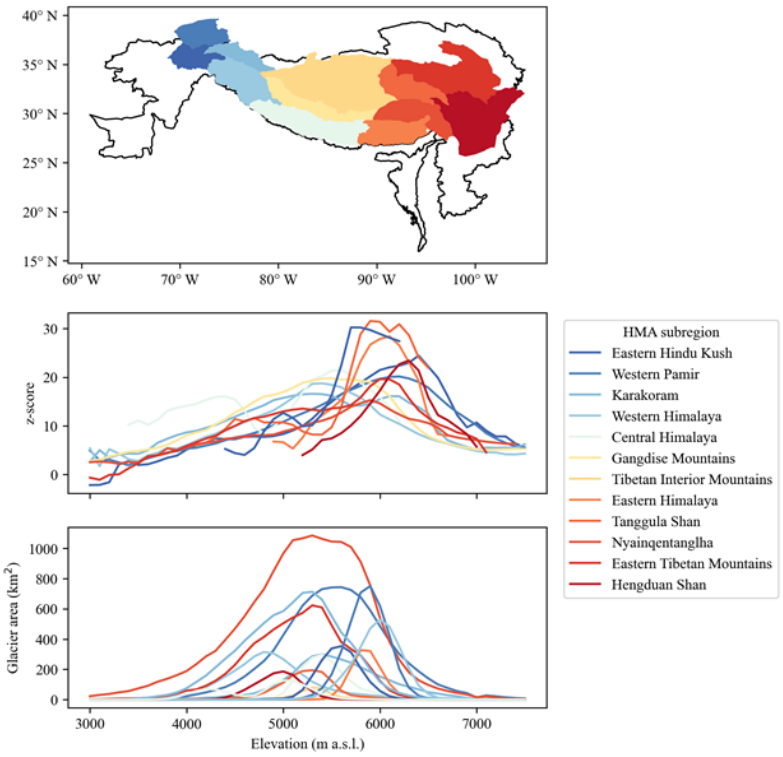

Fig. 3. Figure AR2. Please see text for caption.

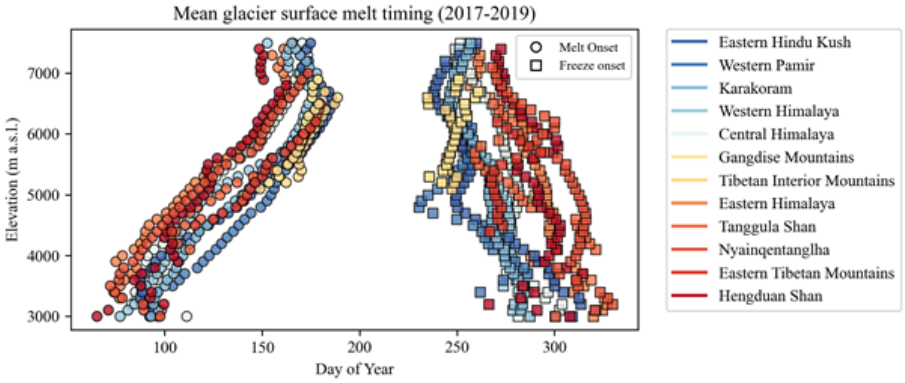

Fig. 4. Figure AR3. Please see text for caption.

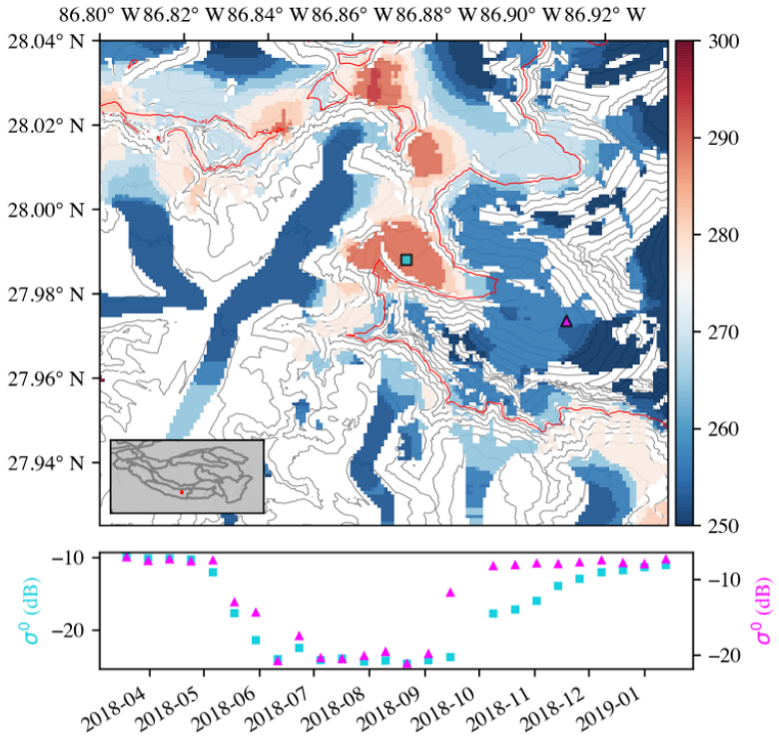

Fig. 5. Figure AR4. Please see text for caption.

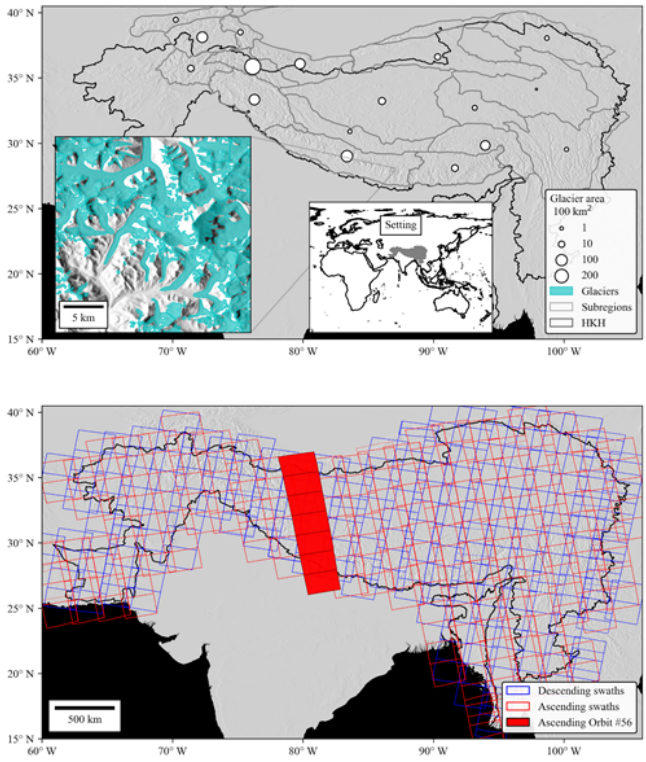

Fig. 6. Figure AR5. Please see text for caption.

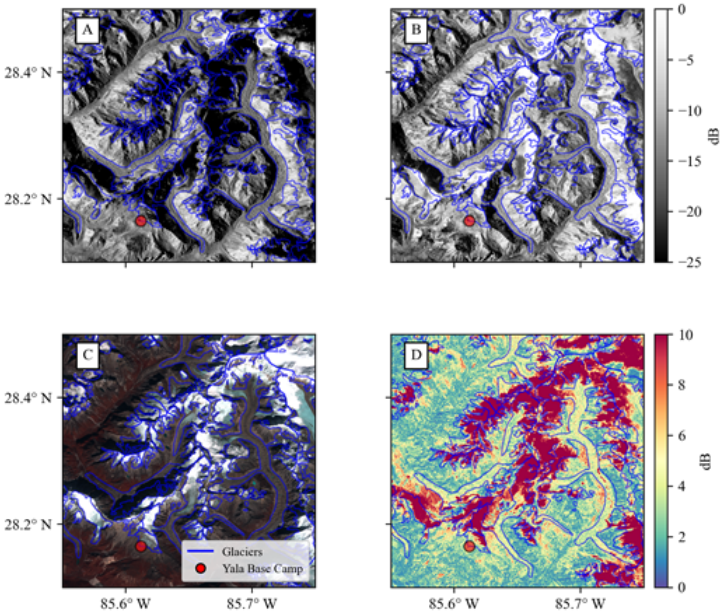

Fig. 7. Figure AR6. Please see text for caption.

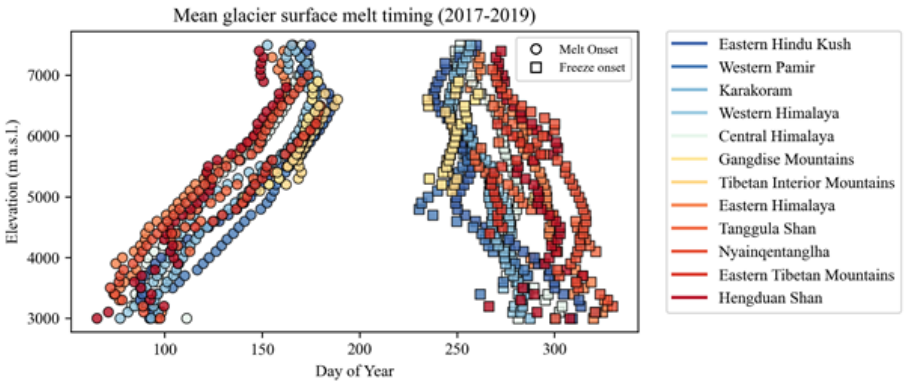

Fig. 8. Figure AR7. Please see text for caption.

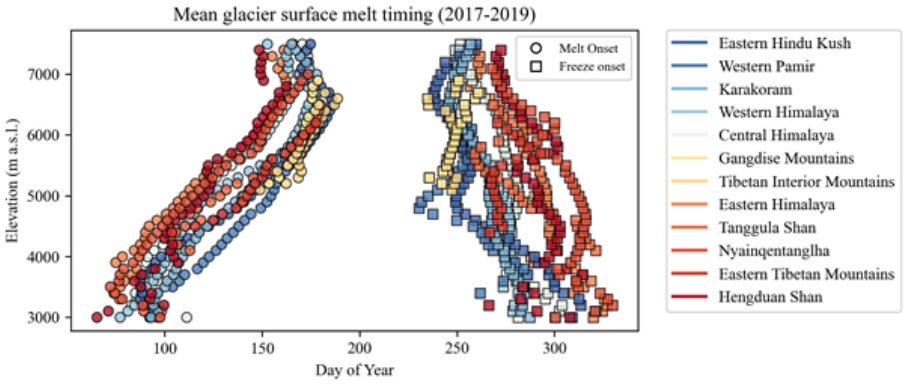

Fig. 9. Figure AR8. Please see text for caption.

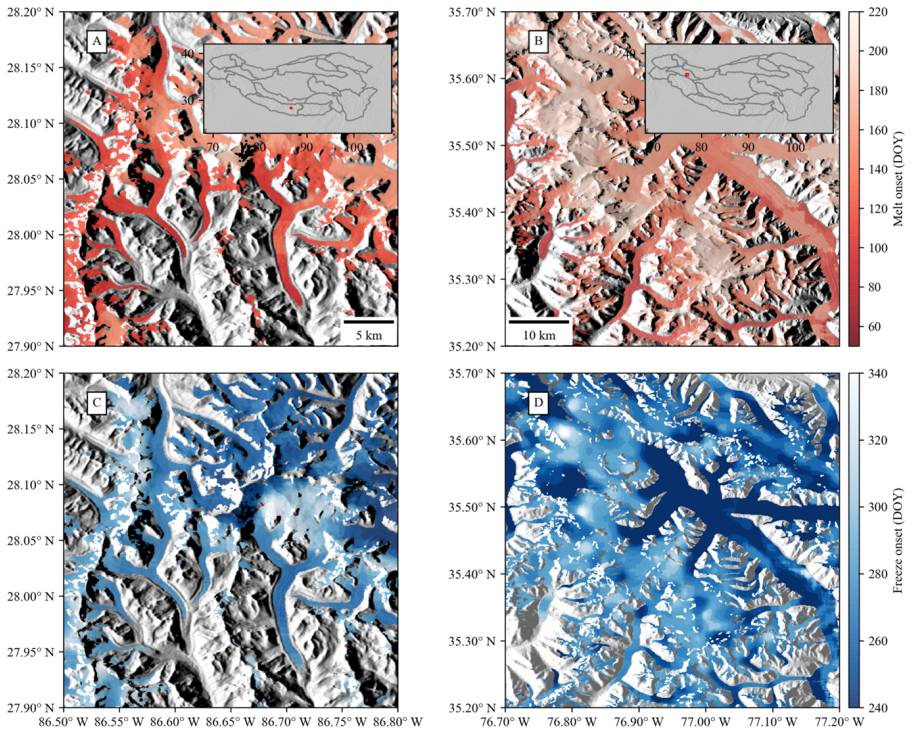

Fig. 10. Figure AR9. Please see text for caption.

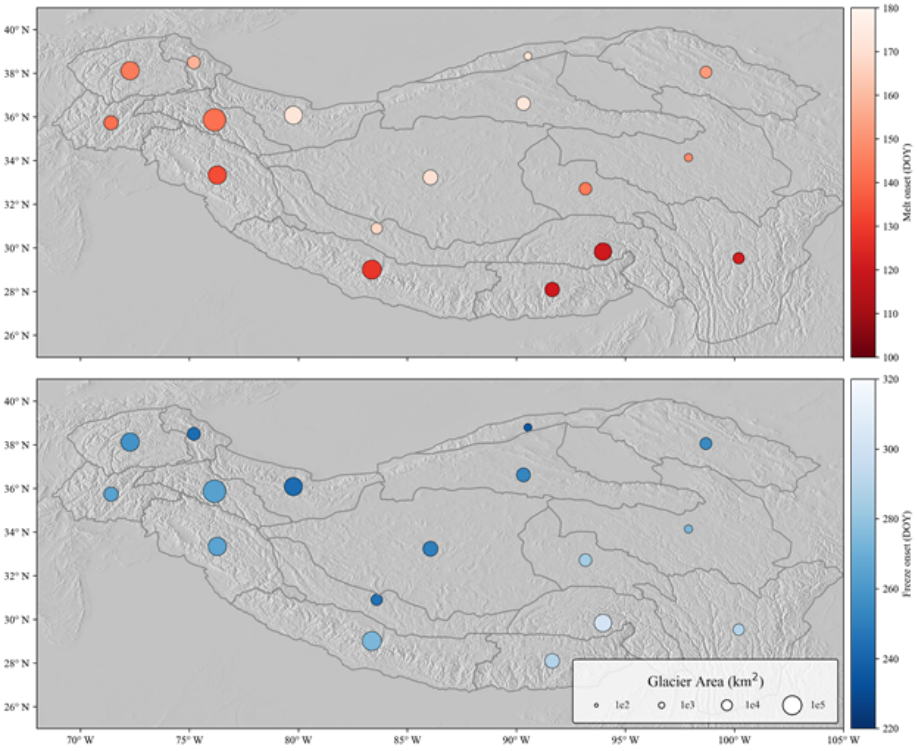

Fig. 11. Figure AR10. Please see text for caption.